applied sciences

MDPI

Article

Influence of FK209 Cobalt Doped Electron Transport Layer in Cesium Based Perovskite Solar Cells

Ahmed Hayali [1,2,*], Roger J. Reeves [2,3] and Maan M. Alkaisi [1,2]

[1] Department of Electrical and Computer Engineering, University of Canterbury, Christchurch 8041, New Zealand
[2] The MacDiarmid Institute for Advanced Materials and Nanotechnology, Wellington 6140, New Zealand
[3] School of Chemical and Physical Sciences, University of Canterbury, Christchurch 8041, New Zealand
* Correspondence: ahmed.hayali@pg.canterbury.ac.nz

Abstract: The efficiency and stability of perovskite solar cells (PSCs) depend not only on the perovskite film quality, but they are also influenced by the charge carriers of both the electron and hole transport layers (ETL and HTL). Doping of the carrier transport layers is considered one of effective technique applied to enhance the efficiency and performance of the PSCs. FK209 cobalt TFSI and lithium TFSI salt were investigated as dopants for mesoporous TiO_2 (M-TiO_2) in the ETL. Herein, FK209 cobalt doping offers improved conductivity, reproducibility and stability compared to other doping or undoped M-TiO_2 control device. It has been found that an optimum concentration of 2.5 mg FK209 cobalt in the M-TiO_2 has resulted in an efficiency of 15.6% on 0.36 cm^2 active device area, whereas, the undoped M-TiO_2 yielded an average efficiency of 10.8%. The enhanced efficiency is due to the improved conductivity of the ETL while maintaining high transparency and low surface roughness with FK209 doping. The M-TiO_2 doped with FK209 has a transparency of the 90% over the visible range and its measured energy gap was 3.59 eV. Perovskite films deposited on the M-TiO_2 doped with FK209 has also a lower PL intensity indicating faster charge extraction. The measured lifetime of the perovskite films deposited on the optimised M-TiO_2 film was 115.8 ns.

Keywords: electron transport layer; titanium dioxide; FK209 cobalt; perovskite solar cells; doping technique

Citation: Hayali, A.; Reeves, R.J.; Alkaisi, M.M. Influence of FK209 Cobalt Doped Electron Transport Layer in Cesium Based Perovskite Solar Cells. *Appl. Sci.* **2022**, *12*, 9382. https://doi.org/10.3390/app12189382

Academic Editor: Antonio Di Bartolomeo

Received: 29 July 2022
Accepted: 14 September 2022
Published: 19 September 2022

1. Introduction

Due to the continued global energy demands, alternative energy sources that are sustainable and less harmful to the environment have been explored. Perovskite solar cells (PSCs) have attracted significant interest owing to their continued improvement in performance and efficiency, use of low cost materials, and simple manufacturing process. During the last decade, the efficiency of the organic-inorganic halide hybrid PSCs has improved from 4% in 2009 [1] to more than 25.6% in 2021 [2]. Since electron transport layer (ETL) plays a significant role in the performance of perovskite solar cells, doping of the ETL is one of the most common approaches and effective strategies used to improve the performance of the PSCs. The ETL has also a significant influence on the morphology, optical properties and consequently on the perovskite film quality. Different materials have been employed in the fabrication of the ETL [3]. However, titanium dioxide (TiO_2) is still the dominant material used in the ETL because of its high transparency, good stability and low cost [4]. The undoped mesoporous TiO_2 (M-TiO_2) possess in-between energy gap defects forming electron traps between the conduction and valence bands due to oxygen vacancy defects, hindering the charge transport extraction and increase in carrier recombination [5,6]. Lithium and FK209 cobalt have been proposed to dope the M-TiO_2 because they improve materials properties using cheap chemicals and easy fabrication process. Many studies have demonstrated that doping TiO_2 with lithium and FK209 cobalt results in a decrease in the carrier recombination, electron traps density, defects and improved the conductivity of the ETL [7–11]. Different strategies have been adopted to

improve the efficiency of the PSCs including increasing the conductivity and transparency of the ETL. In this study, different doping technique to enhance the electrons transfer properties of the M-TiO_2 was investigated. The dopant enables faster electrons transfer and extraction through the M-TiO_2 layer, which leads to improved efficiency of the PSCs.

Tris(2-(1H-pyrazol-1-yl)-4-tert-utylpyridine)cobalt (III) tri[bis(trifluor omethane)sulfoni mide] FK209 Co(III) TFSI salt and Bis(trifluoromethane) sulfonimide lithium salt (TFSI) were investigated as dopant for the M-TiO_2 in the ETL. This is to improve the conductivity and mobility of the ETL and to reduce hysteresis effect. A mixture of lithium and cobalt were prepared and examined to study the influence of this compound on the perovskite carriers lifetime and on the overall device performance.

One of the most common technology employed to enhance the electrons transfer properties of the M-TiO_2 is doping. Doping the ETL results in a decrease in the carrier recombination rate, reduction in the electron traps density, and improve the conductivity of the ETL which consequently decrease the series resistance of the PSC [12]. Numerous articles have been published on doping the ETL with various elements. For example, Liu et al. investigated the effect of using lithium TFSI salt (Li^+) as a dopant for the compact TiO_2. They showed that using Li^+ doped compact titanium dioxide (C-TiO_2) could increase the TiO_2 mobility and reduce the density of electron traps, resulting in increasing the efficiency of PSCs to 17% [7]. In 2018, Sidhik et al. reported on C-TiO_2 prepared using aerosol spray pyrolysis and studied the effect of using FK209 cobalt complex treatment of the M-TiO_2 for ETL [9]. The ETL in Sidhik's study consisted mainly of two layers. The first layer was a blocking TiO_2 and the second layer was M-TiO_2 treated with different concentrations of FK209. This method required two high temperature treatments, the first is performed by holding the sample at 500 °C for 1 h and the second by annealing the sample at 450 °C for 30 min. In the same year, Saliba et al. has demonstrated achieving higher efficiency of 20%, by using M-TiO_2 doped with Li^+ salt deposited on C-TiO_2 prepared using aerosol spray pyrolysis [8]. The aerosol spray pyrolysis technique also requires high temperature treatment by holding the sample at 450 °C.

In 2021, the synthesis of high quality lithium based up-conversion nanoparticles was reported by Alkahtani et al. to expand the spectral absorption and enhance the performance of PSCs. They achieved a PCE of 19%, and a fill factor of 82% [13]. Recently, Alkahtani et al. has fabricated PSCs directly on lithium-based up-conversion thin films of $LiYF_4$ = Yb^{3+}, Er^{3+} and achieved a PCE of 19.1% in comparison to pristine PSCs efficiency of 16.5%. These devices have shown a higher and more stable photovoltaic performance under continuous illumination without a cooling system [14].

In our study, DC-sputtering was used to deposit the C-TiO_2. The DC-sputtering is a well establish technique for high throughput manufacturing environment. It is a low temperature processing, which does not require holding the sample at elevated temperatures as compared with the aerosol spray pyrolysis of C-TiO_2 deposition method. Moreover, the perovskite film reported by Sidhik et al. was based on $MAPbI_3$ ($CH_3NH_3PbI_3$) [9]. We report here on Cesium Lead Iodide $CsI_{0.05}[(FAPbI_3)_{0.85}$ $(MAPbBr_3)_{0.15}]_{0.95}$ based perovskite films. There is no study, to our knowledge that have reported on compact TiO_2 deposited using DC sputtering with the M-TiO_2 layer doped with FK209 cobalt or lithium.

Considerable improvement in the efficiency, fill factor (FF), current density (Jsc) and open circuit voltage (Voc) were observed with doping. Moreover, the stability and reproducibility of the fabricated PSCs are also influenced by doping.

2. Materials and Methods

2.1. Materials

All basic materials were supplied commercially and were utilized as received without any extra purification. Conductive Soda Lime glass fluorine-doped tin oxide (FTO, 12–15 Ω/sq) was sourced from MSE pro^{TM} supplies. Titanium dioxide (TiO_2) paste (30NR-D), formamidinium iodide (FAI), and methylammonium bromide (MABr) were procured from Greatcell solar. Lead (II) iodide (PbI_2) 99.9%, and lead (II) bromide ($PbBr_2$) 99.9% were purchased from

Luminescence technology corp. (Lumtec). Bis(trifluoromethane)sulfonimide lithium salt (Li-TFSI 99.9%), acetonitrile anhydrous, (99.8%), spiro-MeOTAD 99% (HPLC), chlorobenzene (95%), tris(2-(1H-pyrazol-1-yl)-4-tert-butylpyridine)cobalt(III) tri[bis(trifluoromethane)sulfonimide] FK209 Co(III) TFSI salt and 4-tert-Butylpyridine (TBP 98%) were bought from Sigma-Aldrich. Cesium iodide (CsI 99.998%) was purchased from Alfa Aesar. N,N-dimethylformamide (DMF, 99.5%) and dimethyl sulfoxide (DMSO, 99.9%) were acquired from Fisher Scientific, Hampton, NH, USA.

2.2. Methods

A commercially available FTO glass substrate with sheet resistance of 12–15 Ω/sq was used. The FTO glass substrate was etched using zinc powder and hydrochloric acid (2 M) diluted in deionized (DI) water. This step was required to prevent short circuiting during the cell test. Then, substrates were cleaned with acetone, methanol, and isopropanol. Finally, Oxygen plasma was used for 10 minutes to clean substrate and improve the adhesion between the FTO and the compact TiO_2 layer. This is followed by the deposition of 70 nm of compact TiO_2 on the FTO glass substrate using DC-sputtering powered at 200 W [15]. The mesoporous TiO_2 was deposited using spinning coating at a speed of 4000 rpm with acceleration of 2000 rpm/s for 10 s by dissolving 150 mg of TiO_2 paste (30NR-D) in l mL ethanol and stirred at 60 °C for at least 3 h before use. The M-TiO_2 was doped with FK209 cobalt (2.5 mg of FK209 dissolved in 200 µL acetonitrile) and Lithium (2.5 mg of Li^+ dissolved in 200 µL acetonitrile). A 200 µL of the final stock (FK209 or Li) was added to the 1 mL of M-TiO_2 solution. To find the optimum concentration, the concentration of the FK209 cobalt was changed from 1.5 mg to 5 mg and dissolved in 200 µL of acetonitrile. A 150-nanometer thick M-TiO_2 was achieved using a spinner at 4000 rpm with 2000 rpm/s acceleration for 10 s. The M-TiO_2 layer was annealed for half an hour at 450 °C. The perovskite layer was prepared in a glovebox filled with N_2 circulated by two steps spinning. Triple cation perovskite was prepared using FAI (1 M), MABr (0.2), PbI_2 (1.1 M), $PbBr_2$ (0.2 M) in anhydrous dimethylformamide (DMF) and dimethyl sulfoxide (DMSO) were prepared by volume ratio of DMF: DMSO 4:1 (*v*:*v*). The CsI was prepared by dissolving 1.5 M of CsI in DMSO. Following that, a 5% of the CsI was added to the total precursor mixture. The first step in this process was dispensing 100 µL of the triple cation perovskite on the substrates while spinning at a speed of 1000 rpm for 10 s. Then, a second step of spinning at 6000 rpm for 25 s followed by dispensing 230 µL chlorobenzene for 10 s at the end of the rotation and then annealing at 100 °C for 40 min. For the hole transport layer, a 72 mg of spiro-MeOTAD was first dissolved with 1 mL chlorobenzene. Then, a 29 µL of 4-tert-butylpyridine and 18 µL of Li^+ salt were added to the spiro-MeOTAD layer. This was accomplished by using 520 mg of bis(trifluoromethane)sulfonimide lithium salt dissolved in 1 mL of acetonitrile. Finally, 70 nm of gold was deposited as the top electrode using electron beam evaporation.

3. Results and Discussion

3.1. Electrical and Structural Properties of Mesoporous TiO_2 Doped with FK209 Cobalt and Lithium

The use of lithium TFSI salt (Li^+) and FK209 cobalt TFSI salt and a mixture of FK209/Li^+ salt as dopant for the M-TiO_2 ETL layer were investigated. The electronic properties of the doped M-TiO_2 were measured using the van der Pauw technique based on four probes hall measurement system. Table 1 illustrates that the conductivity and mobility of the M-TiO_2 doped with FK209 is much higher than the M-TiO_2 doped with Li^+ salt and higher than M-TiO_2 doped with FK209/Li^+ mixture. This is because the M-TiO_2 doped with FK209 has lower surface roughness which leads to denser films improving the conduction path compared to M-TiO_2 doped with FK209/Li^+ mixture. The electrical properties of the M-TiO_2 doped with FK209 or lithium presented in Table 1 were measured on FTO glass substrate. The conductivity and mobility properties of the control undoped M-TiO_2 are 2.2×10^4 [1/Ω.cm] and 29.3 [cm^2/v.s] respectively [16].

Table 1. Electrical properties of the undoped M-TiO_2 control and M-TiO_2 doped with FK209, FK209/Li^+ and Li^+.

Name	Conductivity (σ) $\times 10^3$ [1/Ω.cm]	Bulk Resistivity (ρ) $\times 10^{-4}$ [Ω.cm]	Mobility (μ) $\times 10^3$ [cm^2/v.s]	Carrier Density $\times 10^{19}$ [cm^{-3}]
M-TiO_2 control	22	0.45	1.23	11.29
M-TiO_2 + Li^+ salt	23.5	0.42	1.73	8.6
M-TiO_2 + FK209 cobalt	30	0.33	8.32	2.27
M-TiO_2 + FK209/Li^+	26.3	0.38	6.2	2.65

The surface morphology of the M-TiO_2 doped with FK209 and Li^+ were studied using atomic force microscopy (AFM). The AFM images in Figure 1 show that the surface of the M-TiO_2 doped with FK209 cobalt has denser grains structure and minimal surface roughness as compared to the M-TiO_2 doped with FK209/Li^+ mixture salt or doped with Li^+. The "root mean square" (RMS) of the surface roughness of the M-TiO_2 layer doped with FK209 shows more homogeneous and smoother surface with an RMS = 16 nm compared to M-TiO_2 doped with Li^+ or doped with FK209/Li^+ which has an RMS value of 25.46 nm and an RMS of 22.75 nm respectively. Figure 1 on the right hand side shows the contact angle measurement of doped and undoped M-TiO_2, and on the left hand side presents the three dimensional AFM imaging for films with the different dopants used and for the undoped M-TiO_2. The x- and y-axes are equal to 1 μm and the z-axis ranges from −0.1 to 0.13 μm. It was found that the surface roughness of the M-TiO_2 doped with cobalt was 16 nm and has the lowest surface roughness compared with lithium doped M-TiO_2 (25.4 nm). This cannot be visualized clearly by just looking at the image only, the Z scale in Figure 1a is 0.08 μm and in Figure 1b,c is 0.09 μm. The appearance of the dark and light areas is not necessarily an indication of actual holes in the structure but rather difference in the heights. This was reflected on the size of the perovskite crystal grains as smoother M-TiO_2 surfaces resulted in larger perovskite grain size [9], as shown in Figure 2 histogram. Surface wettability (hydrophilicity) was investigated using the contact angle (θ) value between DI water droplet and a surface. The surface is more hydrophilic, if DI water droplet on the surface is more flat with small contact angle value. It can be observed from Figure 1 that the contact angle of the undoped M-TiO_2 control sample is higher than the M-TiO_2 layer treated with other dopants. It is found that doping with lithium or cobalt employed in this study resulted in a reduction in contact angle and has increased surface hydrophilicity compared to pristine sample. There is significant difference in the contact angle of undoped M-TiO_2 (θ = 14°) compared to M-TiO_2 doped with FK209 (θ = 4.2°), an indication of the improved wettability of TiO_2 layer. This could be due to the reduction of the surface roughness of the layer. Hence, by doping the M-TiO_2 with FK209, a more hydrophilic surfaces were achieved.

It is found that the surface roughness of the ETL influences the grains size and topography of the perovskite film as it acts a seeding substrate during the deposition of the perovskite active layer [9]. In addition, the interface between the ETL and active perovskite film is also affected. Perovskite films with large grains size has produced lower series resistance of the active layer, leading to improvement in the performance of PSCs [17]. Recent researches have shown that the existence of large-sized perovskite grains enhance the mobility of charge carrier and decreases recombination of bulk defects [18,19]. The highest conversion efficiency in this study was achieved using M-TiO_2 doped with FK209 due to its lowest surface roughness and largest grains size perovskite films.

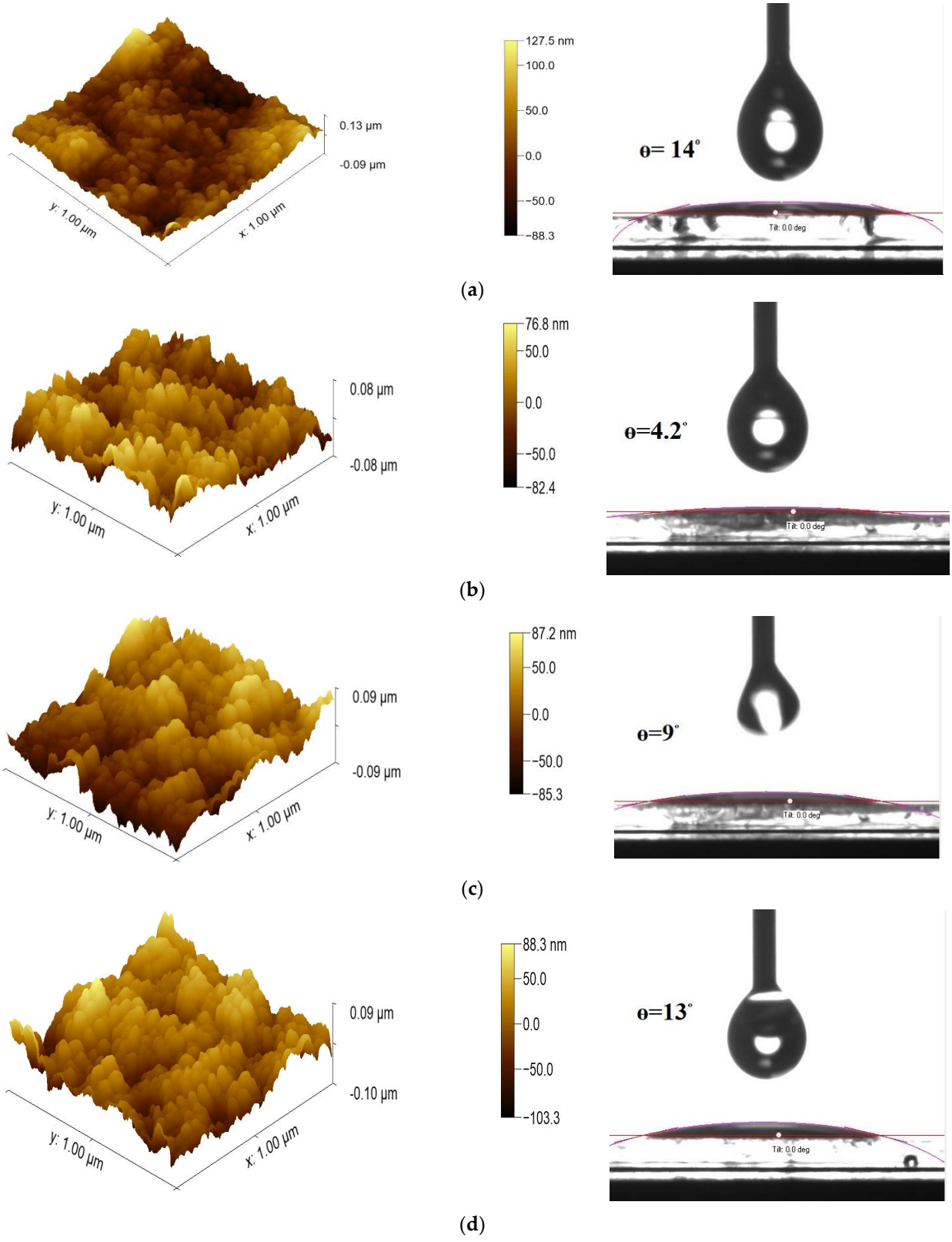

Figure 1. Left, AFM images of the surface morphology structure and roughness of the (**a**) undoped mesoporous TiO_2, RMS = 34.5 nm; (**b**) M-TiO_2 doped with FK209, RMS = 16 nm; (**c**) FK209/Li^+, RMS = 22.75 nm; (**d**) Li^+, RMS = 25.46 nm. Right, contact angle measurement of (**a**) undoped M-TiO_2, θ = 14°; (**b**) M-TiO_2 doped with FK209, θ = 4.2°; (**c**) FK209/Li^+, θ = 9°; (**d**) Li^+, θ = 13°.

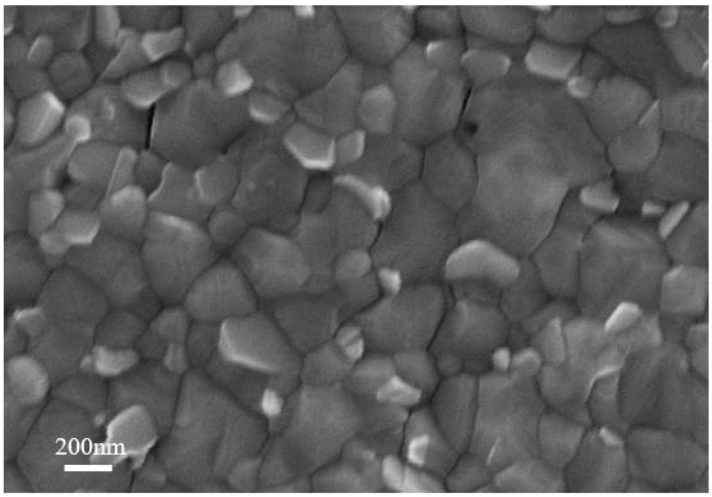

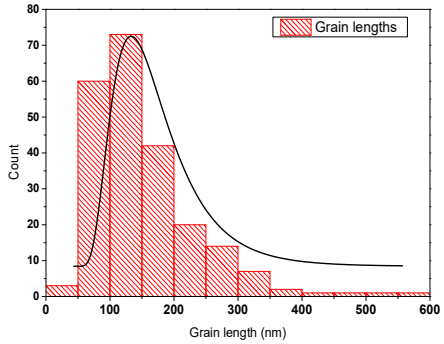

(**a**)

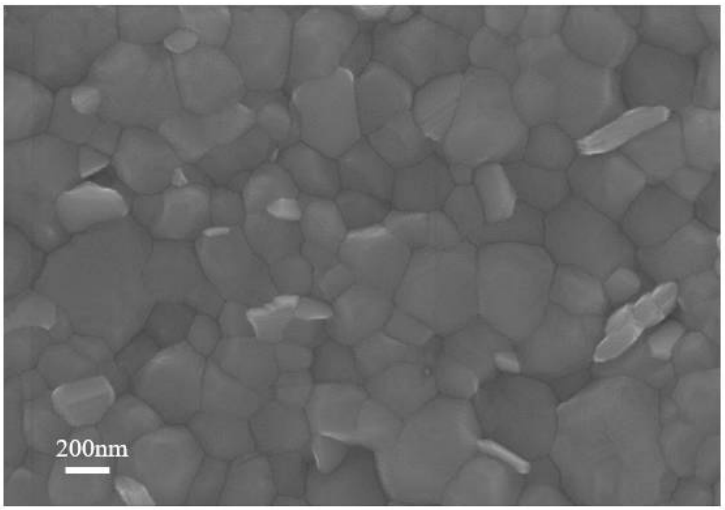

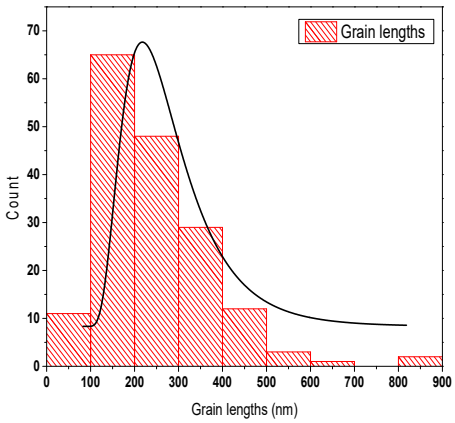

(**b**)

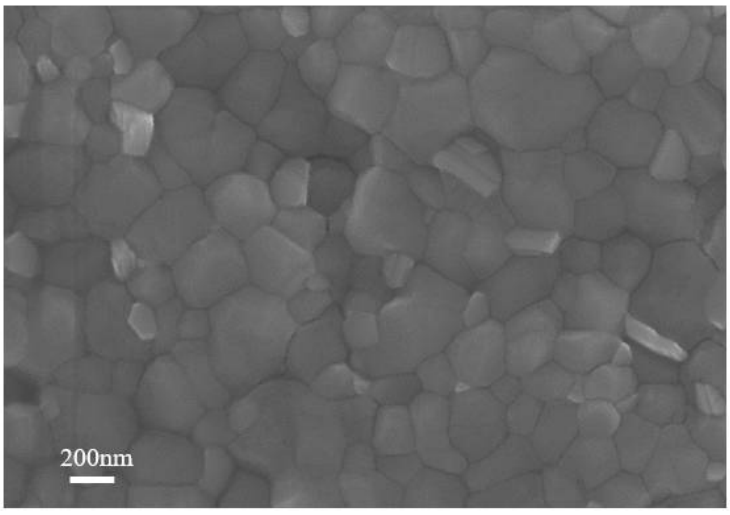

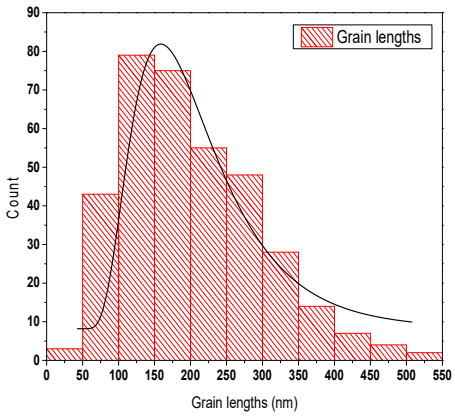

(**c**)

Figure 2. *Cont*.

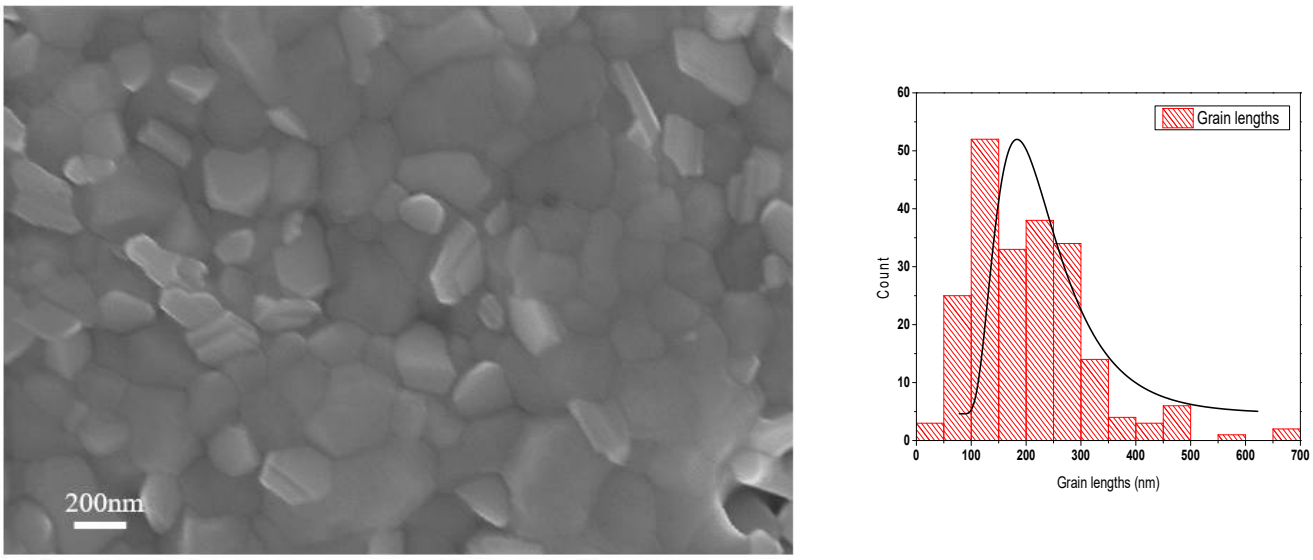

(**d**)

Figure 2. Left, SEM images of surface topography of the perovskite layer deposited on the (**a**) undoped M-TiO_2 and mesoporous TiO_2 doped with (**b**) FK209, (**c**) FK209/Li^+ and (**d**) Li^+. Right, the histogram shows an average grains size for (**a**) undoped M-TiO_2, 163.9 nm; (**b**) M-TiO_2 doped with FK209, 242 nm; (**c**) FK209/Li^+, 210 nm; (**d**) Li^+, 205 nm.

ImageJ software was used to calculate the grains size and Origin9 software was used to plot their histogram. The SEM images in Figure 2 show that using M-TiO_2 doped with FK209 provides a uniform perovskite films with an average grains size of 242 nm, which is larger than grains size of perovskite deposited on M-TiO_2 doped with Li^+ or FK209/Li^+. The average grains size of perovskite deposited on M-TiO_2 doped with FK209/Li^+ decreased to 210 nm, whereas, perovskite films deposited on M-TiO_2 doped with Li^+ has an average grains size of 205 nm as shown in the histogram of Figure 2. Our results demonstrate that perovskite deposited on M-TiO_2 doped with FK209 have the largest grains size and possess less defects compared with perovskite deposited on ETL with the other dopants. Larger grains results in a dense structure and improved crystallization allowing for enhanced conduction properties [20].

3.2. Optical Properties of Mesoporous TiO_2 Doped with FK209 Cobalt and Lithium

The transparency of the ETL is another factor that influences the efficiency of perovskite solar cells. High transparency and high conductivity are essential requirements in the function of the ETL. The transparency of undoped mesoporous TiO_2 is round 90% [16]. In this study, the FK209 was used to dope the M-TiO_2 film to increase its conductivity but without reducing its transparency significantly. The conductivity has increased from 22×10^3 to 30×10^3 [1/Ω.cm] while the transparency was maintained its value around 90% at 600-nanometer wavelength. To study the influence of doping on the transparency of the ETL, M-TiO_2 was doped with FK209, lithium and a mixture of FK209/Li^+. An Ultraviolet-Visible spectrometry (Cary 6000i) measurement was utilized to measure the transparency of the ETL films. Generally, it is clear from Figure 3 that 85% transparency have been obtained from all M-TiO_2 films doped with FK209, Li^+ or FK209/Li^+ over the visible wavelength range. There is slight increase in the transparency between 300–500 nm and 650–800 nm for the M-TiO_2 doped with FK209 compared to M-TiO_2 doped with lithium or FK209/Li^+. Figure 4 shows the absorbance of the M-TiO_2 doped with FK209, Li^+ or FK209/Li^+ measured using Cary UV-Vis spectrometer. There is a weak absorption between 350–800 nm, and much higher absorption at a range from 300–350 nm.

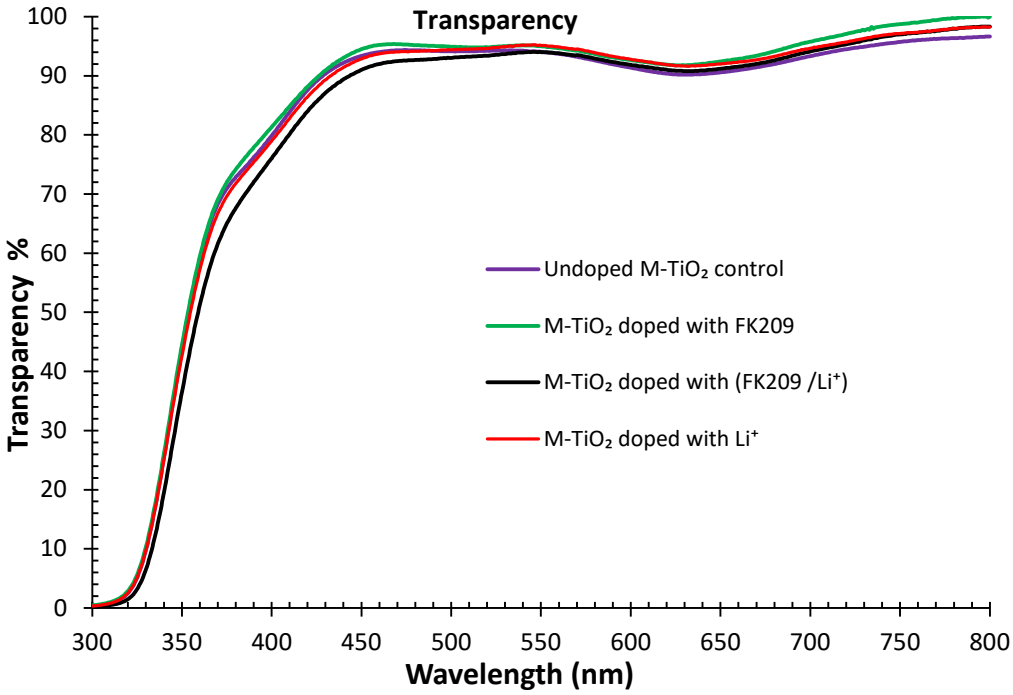

Figure 3. Optical transparency properties of mesoporous TiO_2 doped with FK209, FK209 /Li^+, and Li^+.

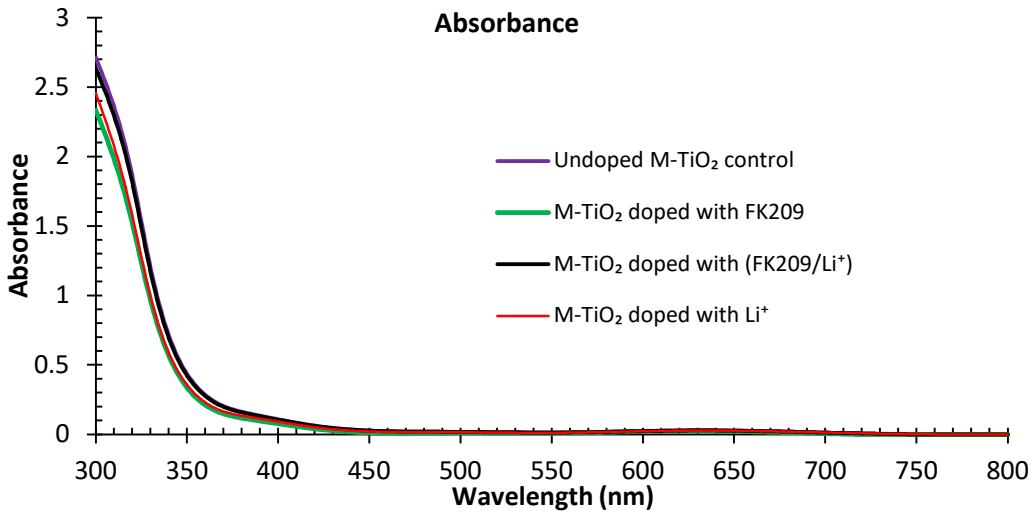

Figure 4. Optical absorbance properties of mesoporous TiO_2 doped with FK209, FK209 /Li^+, and Li^+.

The optical band gap energy of the films can be extrapolated from the absorption data using Tauc plot method [21]. Figure 5 displays the extracted energy band gaps of the un-doped M-TiO_2 and M-TiO_2 doped with FK209, FK209/Li^+ and Li^+. The Tauc plot was obtained from the absorption spectra shown in Figure 4. An extrapolation technique (dotted lines) was used to determine the optical band gap of the M-TiO_2 doped with different dopants. The energy gaps of the undoped M-TiO_2 and M-TiO_2 doped with FK209, FK209/Li^+ or Li^+ are 3.55 eV, 3.59 eV, 3.56 eV, and 3.58 eV respectively. A number of studies have shown that the energy gap of the un-doped M-TiO_2 is around 3.5 eV in agreement with our results [16,22,23].

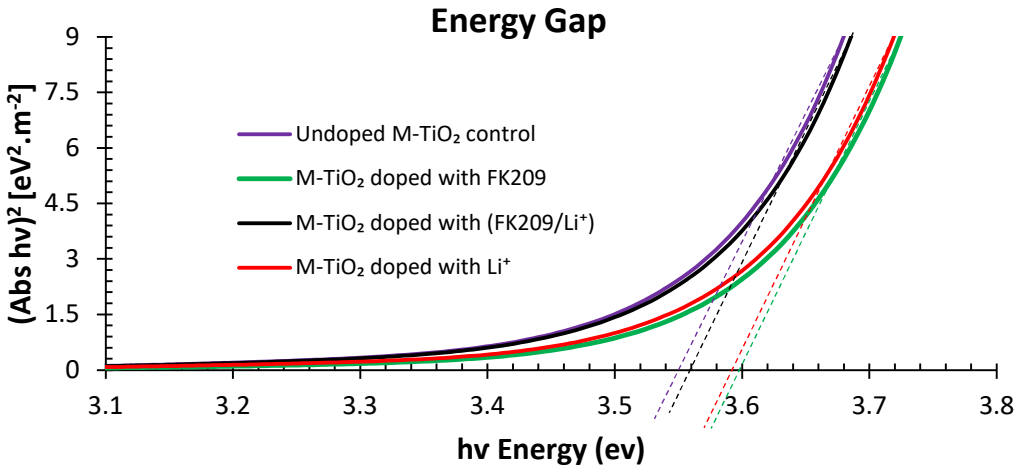

Figure 5. Extrapolation of the energy gap of M-TiO_2 doped with FK209, FK209 /Li^+, and Li^+, using Tauc plot.

Figure 6 shows the absorption of the perovskite films deposited on undoped M-TiO_2 and M-TiO_2 doped with FK209, FK209/Li^+ and Li^+ measured over the 440 nm to 800 nm range. It is observed that the perovskite films deposited on M-TiO_2 doped with FK209 has the same absorbance spectrum compared with perovskite deposited on M-TiO_2 doped with FK209/Li^+ or Li^+. However, there is a slight improvement of around 5% in absorption spectrum between 500–800 nm. This could be one of the reasons for the increased current density obtained for the perovskite film deposited on the M-TiO_2 doped with FK209 [6]. As a result, the PSCs prepared with ETL doped with FK209 have produced the highest efficiency. The absorbance spectra of our perovskite samples were in agreement with other reported study [24].

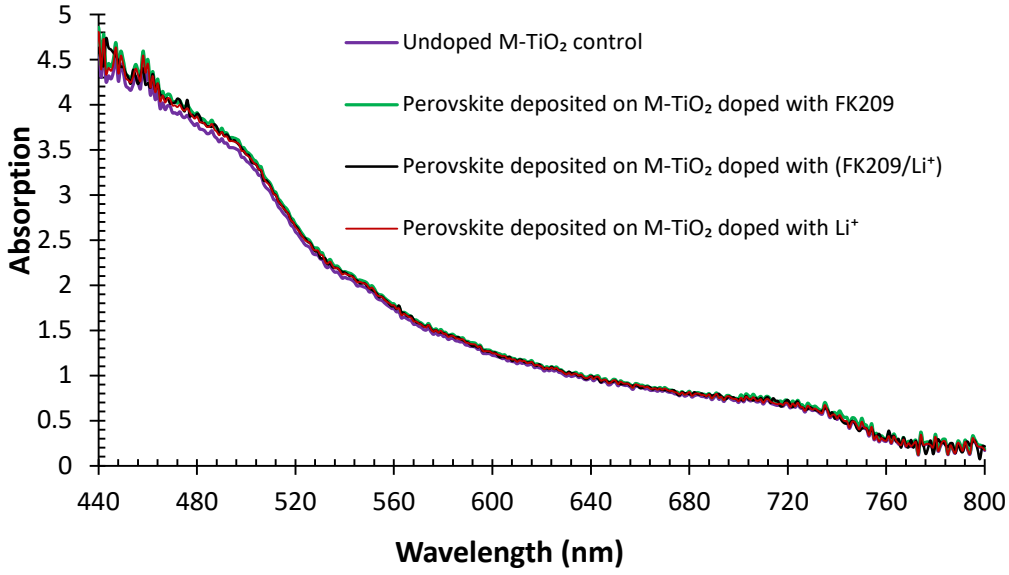

Figure 6. Absorption of perovskite film deposited on M-TiO_2 doped with FK209, FK209/Li^+ and lithium.

Figure 7 shows the relation between hv (ev) and (Abs hv)^2. Where, hv is the incident photon energy and Abs is absorption of film. The energy gap of the perovskite film deposited on M-TiO_2 doped with FK209, FK209/Li^+ and Li^+ is measured around 1.6 eV. Hence, there is no large shift in energy gap of perovskite active layer with changing the ETL dopant as expected. These results confirm that the active perovskite layer deposited on the M-TiO_2 doped with the studied dopants is not affected by the dopant type of the ETL [25].

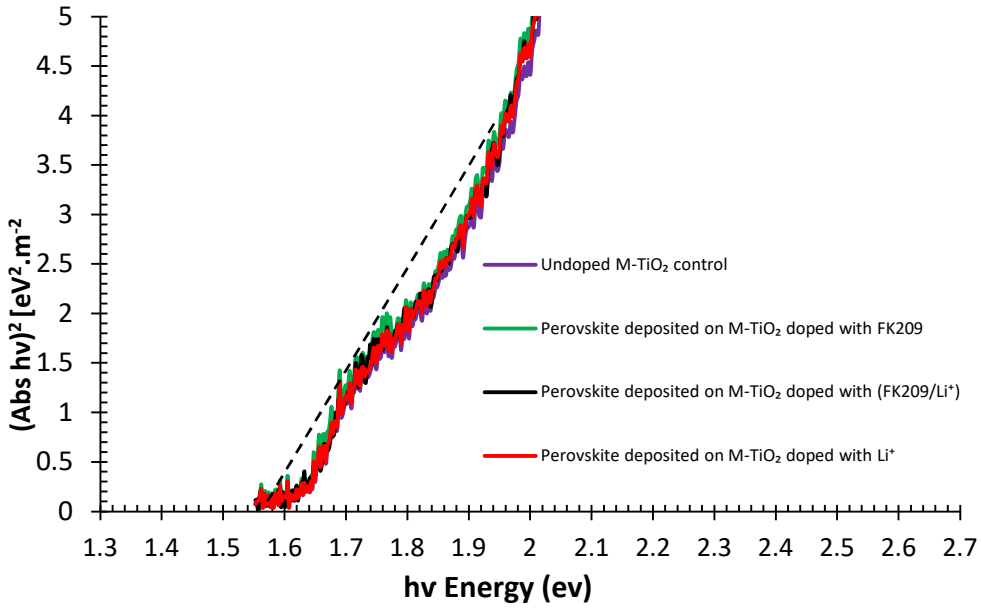

Figure 7. Energy gap of perovskite films deposited on M-TiO_2 doped with FK209, FK209/Li^+ and lithium, using Tauc plot.

The photoluminescence (PL) spectra of perovskite films deposited on M-TiO_2 doped with FK209, FK209/Li^+ or lithium are shown in Figure 8. It can be observed that the perovskite films deposited on undoped M-TiO_2 or on M-TiO_2 doped with FK209/Li^+ or on Li^+ have a higher PL intensity, indicating the existence of strong recombination in the perovskite active layer [16,26]. A peak emission at 775 nm have been obtained for all perovskite films deposited on doped or undoped M-TiO_2. The PL spectra showed a lower intensity for perovskite film deposited on M-TiO_2 doped with FK209, indicating that faster charge extraction at the interface layer occurs before their recombination [9]. This implies that the M-TiO_2 doped with FK209 improves the interface layer and increases charge extraction from the active perovskite layer. Consequently, this prevents carrier charge recombination, resulting in improved short circuit current Jsc, open circuit voltage Voc and fill factor FF of the PSC because of the passivation of oxygen defects at the interface layer [9].

Figure 9 shows the PL decay time of the perovskite films deposited on various ETL coated substrates; M-TiO_2 doped with FK209, FK209/Li^+ and Li^+. In principle, electrons generated in the active perovskite layer transfer to the ETL before recombination occurs in the perovskite film [16,26]. This is due to the fact that long carrier lifetime lead to an enhancement in charge transfer and extraction of electrons. The charge carrier lifetime (τ) of the PL decay signals can be estimated by fitting the dynamic exponential curve expressed as:

$$Y = Y0 + A1 \times \exp\left(\frac{-t}{\tau}\right) \quad (1)$$

where, $A1$ is the time independent coefficient of the amplitude fraction, τ is decay time, Y0 is a constant. The measured lifetime of the perovskite films deposited on the M-TiO_2 doped with FK209 was 115.8 ns as compared to 113.4 ns for perovskite deposited on the M-TiO_2 doped with lithium and 120.9 ns for M-TiO_2 doped with FK209/Li^+. This results indicating more efficient charge transfer and better electrons extraction can be obtained with a mixture of FK209/Li^+. The PL measurements also demonstrate that FK209 cobalt is more suitable dopant to the M-TiO_2 compared with Li^+.

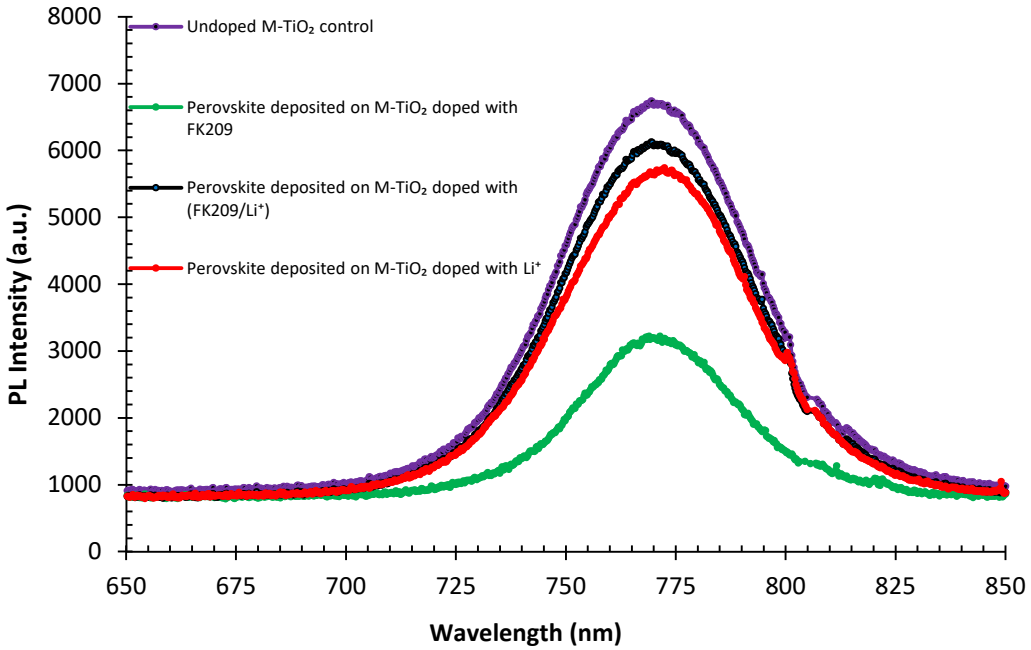

Figure 8. Photoluminescence spectra of perovskite films deposited on M-TiO_2 doped with FK209, FK209/Li^+ and lithium.

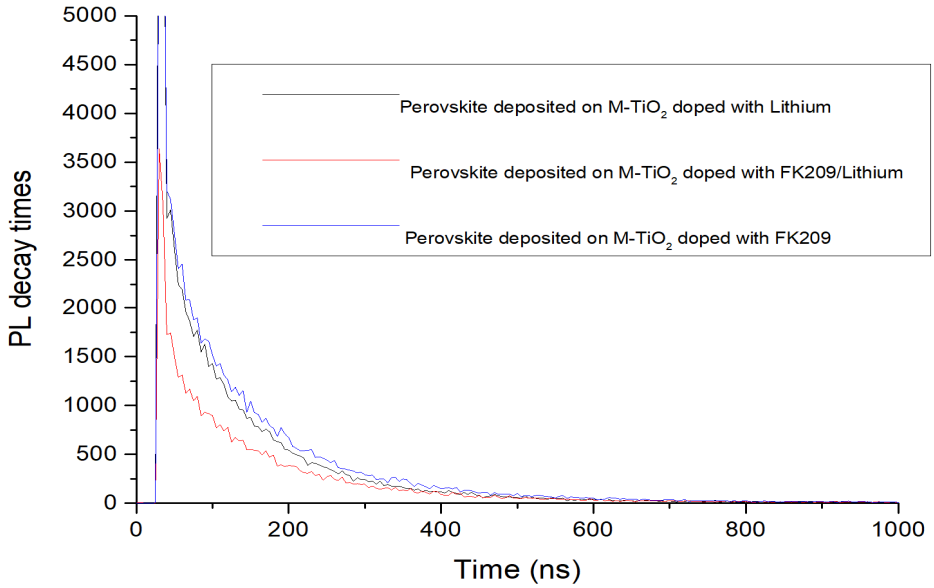

Figure 9. Photoluminescence decay time of perovskite deposited on M-TiO_2 doped with FK209, FK209/lithium and lithium and measured using fluorescence PL decay lifetime.

3.3. Device Characterization

Figure 10 left, illustrates the main structure of the PSC device and on the right is a photograph of the PSC fabricated in this work. The current density-voltage (J–V) characteristics curves of the PSCs were obtained by employing an ABET Sun3000 sunlight simulator set at AM 1.5 G (100 mW/cm^2). The overall sample size was 2.5 × 2.5 cm^2.

The different layers of the PSC are illustrated in Figure 11. It shows a detailed schematic structure of a typical device composed of FTO/C-TiO_2/M-TiO_2 doped with FK209 as the ETL/Perovskite $CsI_{0.05}[(FAPbI_3)_{0.85}$ $(MAPbBr_3)_{0.15}]_{0.95}$/Spiro-MeOTAD as the HTL and an Au back electrode. Figure 11 illustrates an SEM of a cross-section of the complete perovskite solar cell. The optimized perovskite solar cell comprises of a 70-namometer thick C-TiO_2 layer and a 150-nanometer thick M-TiO_2 doped with FK209 cobalt film. The

active perovskite layer thickness was 350 nm, followed by a 180-nanometer thick spiro-MeOTAD, and finally a 70 nm of the electron beam evaporated gold as the backside electrodes for the complete solar cell device.

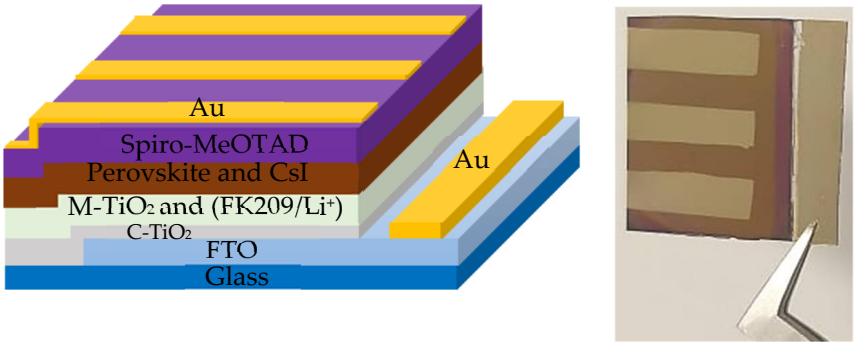

Figure 10. Left, schematic structure of the perovskite solar cell. Right, photograph of 2.5 × 2.5 cm^2 PSC fabricated in this study.

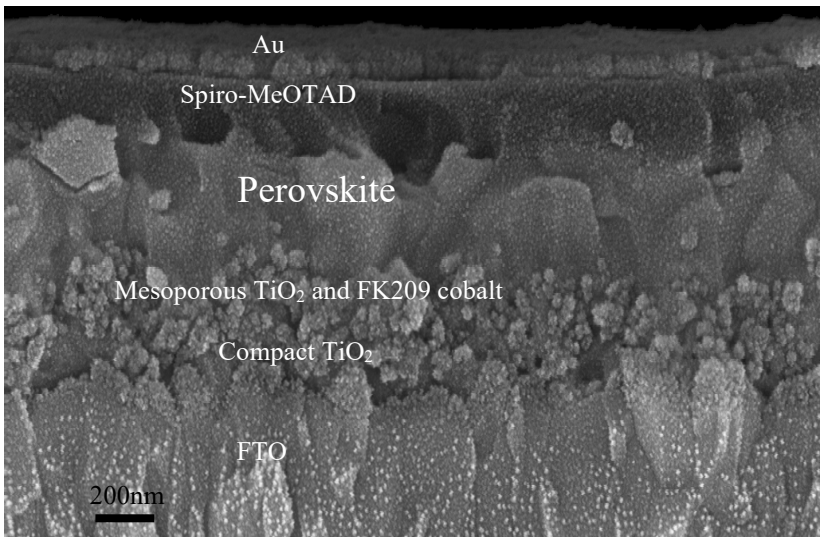

Figure 11. An SEM image of the cross-section of the perovskite solar cell device fabricated in this study showing the different layers.

3.4. Current Density-Voltage (J–V) Characteristics

All the illuminated current density-voltage characteristics of the PSCs were measured using (ABET Sun3000) with AM 1.5 G sunlight simulator with an average light intensity of 100 mw/cm^2. An Abet technology model 15,150 reference cell with KG5 filter traceable to NIST, NREL, Fraunhofer ISE and ISPRA standard artefacts were employed to certify our efficiency measurements. In this work, the overall samples size was 2.5 × 2.5 cm^2 with an active device area of 0.36 cm^2. The active area is defined by the area of the window opening on the otherwise masked backside of the glass substrate. The cells were exposed to sunlight simulator though this window. Measured value of our active device area is 0.36 cm^2, which is larger than most of the reported areas in the literatures [8,16,17]. This indicates the potential of scaling up attributed to the use of $CsI_{0.05}$ $[(FAPbI_3)_{0.85}$ $(MAPbBr_3)_{0.15}]_{0.95}$ instead of MAI ($CH_3NH_3PbI_3$) and the processes followed in this work [9].

To ensure reproducibility, 15 samples were fabricated using M-TiO_2 doped with FK209 cobalt and 10 samples using un-doped M-TiO_2 and M-TiO_2 doped FK209/Li^+ or lithium. Figure 12 shows the (J–V) characteristic curves of the perovskite solar cells. All key solar cells electrical parameters are shown in Table 2. The solar cell prepared with perovskite deposited on M-TiO_2 doped with FK209 yielded the highest efficiency of 15% in the forward sweep and 16.3% backward sweep. There is a noticeable increase of 14%

in Voc in the perovskite film deposited on M-TiO_2 doped with FK209 as compared to the perovskite deposited on M-TiO_2 doped with Li^+. The fill factor (FF) have significantly increased by 18.5% in the perovskite deposited on M-TiO_2 doped with FK209 compared to perovskite deposited on un-doped M-TiO_2 control. The significant improvement of both the FF and Voc is attributed to the increase in conductivity of the ETL and reduction of the device series resistance. The FF have increased by 13.5% in the perovskite films deposited on M-TiO_2 doped with FK209 compared to perovskite deposited on M-TiO_2 doped with FK209/Li^+ or Li^+. The improvement in the FF is attributed to the drop in the series resistance of the solar cell from 12 to 9.3 $\Omega.cm^2$ [27]. The combined resistance of the transparent conductive oxides used for the electrodes and the active perovskite film results in a series resistance Rs that significantly influence the fill factor and the efficiency of the solar cell. In perovskite solar cells, the conductivity of the transparent conductive oxide can be enhanced by increasing the film thickness, but this will lead to decrease in the transparency, which impact the cell performance. This has limited our fill factor to 56%. Our results showed an average Rs, of 9 $\Omega.cm^2$ for cobalt doped TiO_2, and 15 $\Omega.cm^2$ for un-doped M-TiO_2. A compromise has to be reached between transparency and conductivity to achieve higher fill factor, this is beyond the scope of this study. Moreover, we are using FTO glass substrate with sheet resistance of 12–15 Ω/sq while the reported FTO coated glass substrate has a sheet resistance of 8 Ω/sq [17]. This might also added to the increased value of Rs found in this study. When we compare our average series resistance with others reported, it is in agreement with other published work [7,28]. The average power conversion efficiency (PCE) of the perovskite cell deposited on M-TiO_2 doped with FK209 has improved by 28% compared to perovskite deposited on M-TiO_2 doped with Li^+. There are slight variations found in the short circuit current density between all cells prepared with different dopants and the average Jsc was 26 mA/cm^2 in forward and backward scanning. It is widely accepted in the literature that the backward scanning gives higher efficiency than forward scanning. This is related to a phenomenon called J−V hysteresis. It is due to charge distribution effect when applying external electric field. It relates to slow transient capacitive current, charge carriers trapping, ion migration and ferroelectric polarization, which can also cause band bending [29–31].

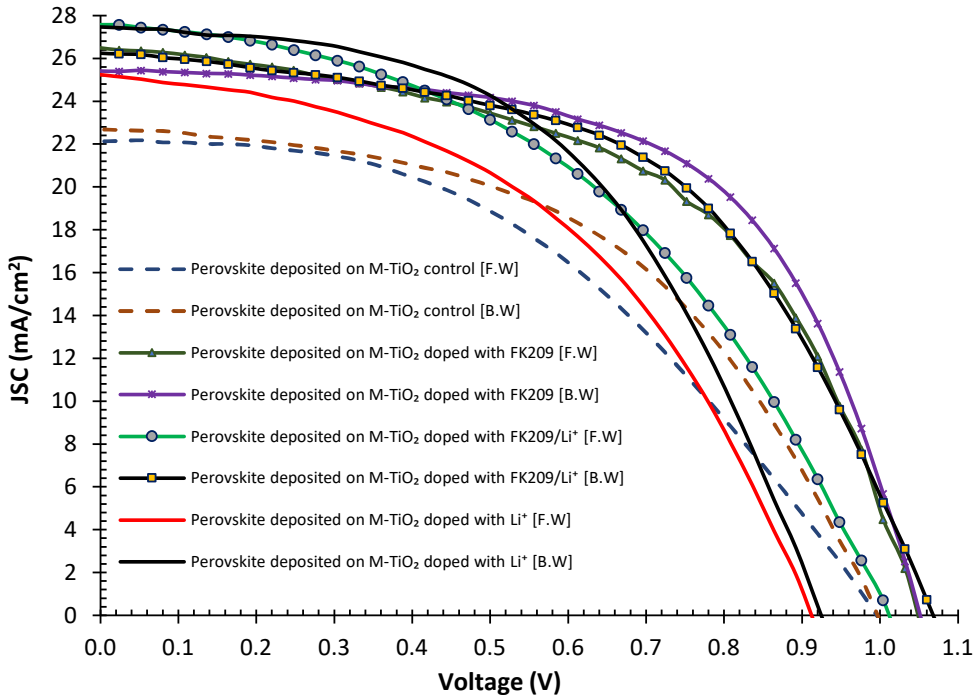

Figure 12. The illuminated J-V characteristic curves of perovskite solar cells deposited on ETL of M-TiO_2 doped with FK209, FK209/Li^+ and lithium.

Table 2. Perovskite solar cell key parameters measured for the different dopants investigated in this study. It is showing the average value for each set of parameter.

Sample Description	Sweep Direction	EFF%	FF%	Voc [mV]	Jsc [mA/cm^2]	Vmax [mV]	Jmax [mA/cm^2]	Isc [mA]	R_{shunt} [Ω.cm^2]	R_{series} [Ω.cm^2]
M-TiO_2 Control	Forward	10	44.8	996	22.1	584	16.8	7.9	1224	18
	Backward	11.6	50	997	22.6	668	17	8.2	1289	12
	Average	10.8	47.4	996.5	22.3	626	16.9	8.05	1256	15
M-TiO_2 doped with FK209	Forward	15	53	1049	26.4	724	20.3	9.4	1305	9.7
	Backward	16.3	59.5	1052	25.4	780	20.4	9.07	2024	9
	Average	15.6	56.2	1050	25.9	752	20.3	9.2	1664	9.3
M-TiO_2 doped with FK209/Li^+	Forward	13	45.4	1011	27.1	640	19.8	9.8	1249	14
	Backward	15.4	53.6	1060	26.2	724	20.7	9.3	3048	13.6
	Average	14.2	49.5	1035	26.9	682	20.2	9.5	2148	13.8
M-TiO_2 doped with Li^+	Forward	11	47.1	912	25.2	584	18.5	9	981	12.9
	Backward	13.3	51	925	26.8	612	20.9	9.8	1105	12.6
	Average	12.1	49	918	26	598	19.7	9.4	1043	12.7

3.5. Optimization of the FK209 Cobalt TFSI Concentration in Mesoporous TiO_2

The highest efficiency of the PSCs was achieved with the M-TiO_2 layer doped with FK209 cobalt. Optimization of the FK209 concentration was performed to achieve best overall device performance. Table 3 shows that the M-TiO_2 layer doped with 2.5 mg of FK209 has highest conductivity (lower resistivity) and has higher mobility compared to M-TiO_2 prepared with dopant concentration of 1.5-mg or 5-mg. The improved properties obtained with 2.5 mg concentration is due to changes in crystal formation and grain size which affect the surface roughness and wettability of the material.

Table 3. Electrical properties of the M-TiO_2 doped with different concentrations of FK209.

Name	Conductivity (σ) $\times 10^3$ [1/Ω.cm]	Bulk Resistivity (ρ) $\times 10^{-4}$ [Ω.cm]	Mobility (μ) $\times 10^3$ [cm^2/v.s]	Carrier Density $\times 10^{19}$ [cm^{-3}]
M-TiO_2 doped withFK209 (1.5 mg)	23	0.42	3.2	4.6
M-TiO_2 doped with FK209 (2.5 mg)	30	0.33	8.32	2.27
M-TiO_2 doped with FK209 (5 mg)	27	0.37	4.8	3.52

It is clear from Figure 13 that the transparency of the M-TiO_2 doped with FK209 is more than 85% at 400 nm and over the entire visible wavelength range. There is not much variations in transparency with the doping concentration used; 1.5 mg, 2.5 mg or 5 mg. However, there is a slight increase in the transparency between 450–700 nm for the M-TiO_2 doped with 2.5 mg of FK209 compared to other concentration of FK209. Figure 14 shows the absorbance of the M-TiO_2 doped with different concentrations of FK209 measured using Ultraviolet-Visible spectrometry (Cary 6000i). As expected, there is small absorption (10–15%) between 450–800 nm wavelengths range, and much higher absorption between 300–350 nm wavelengths.

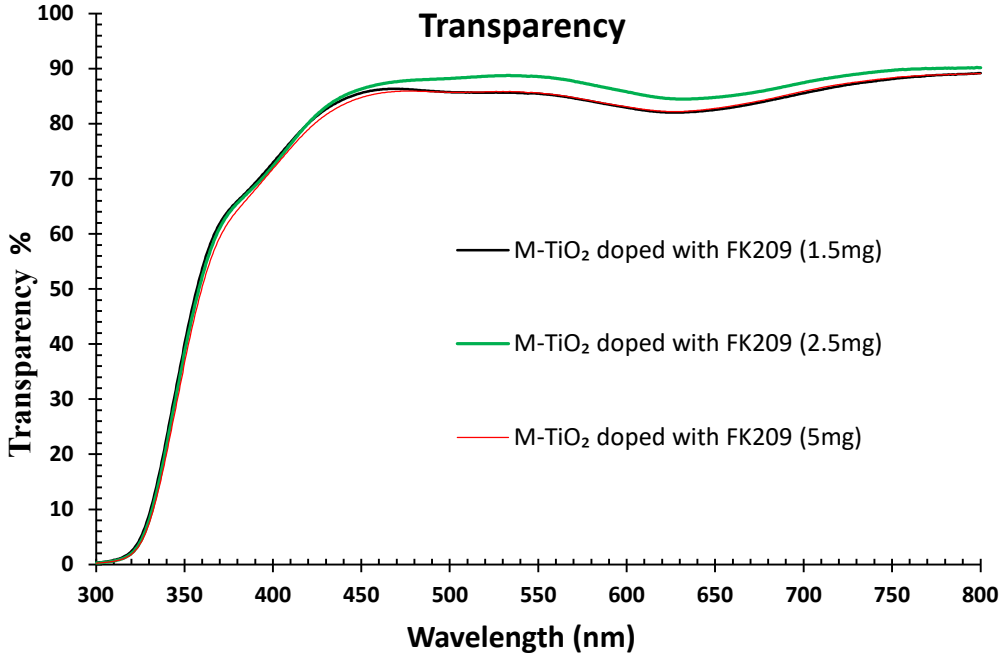

Figure 13. Transparency of the M-TiO_2 doped with 1.5-mg, 2.5-mg and 5-mg concentrations of FK209 cobalt.

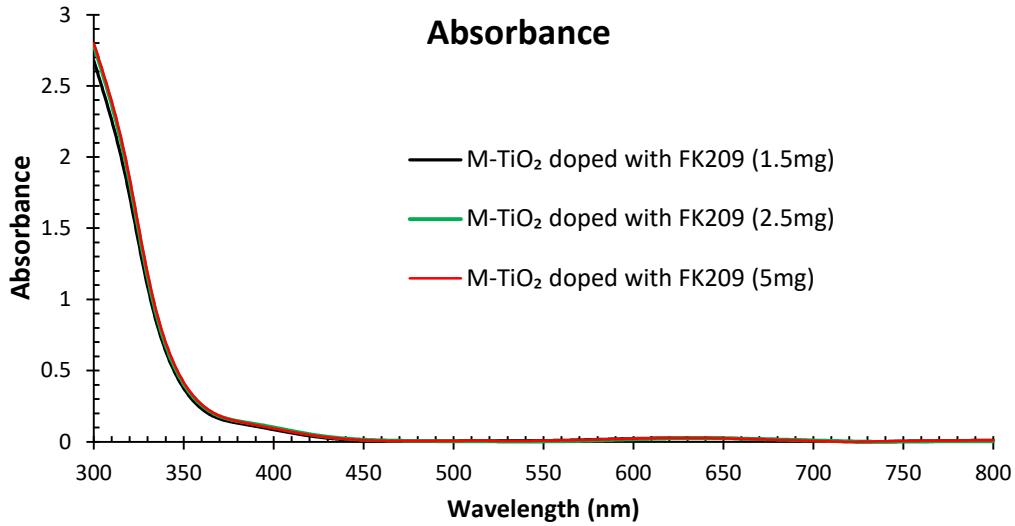

Figure 14. Absorbance spectrum of the M-TiO_2 doped with 1.5-mg, 2.5-mg and 5-mg concentrations of FK209 cobalt.

The energy gap of the M-TiO_2 film can be extrapolated from the absorption data using Tauc plot [21]. Figure 15 illustrates the relationship between hv (ev) and $(Abs\ hv)^2$ for the film. The energy gap of the M-TiO_2 doped with FK209 at 1.5-mg, 2.5-mg and 5-mg concentration deduced from the plot were 3.6 eV, 3.59 eV and 3.56 eV respectively.

To evaluate the reproducibility of the ETL deposition and doping process, 30 samples were prepared and tested. Figure 16 illustrates the efficiency statistic histogram for devices fabricated using compact TiO_2 prepared employing DC-sputtering as a first layer in the ETL followed by an M-TiO_2 doped with various concentrations of FK209. The PCE of the PSCs deposited on M-TiO_2 doped with 2.5 mg FK209 is ranging between (12.5–15.5)% and displaying narrower distribution compared to the ones prepared with 1.5 mg and 5 mg concentration. For example, the PCE of the PSCs fabricated using M-TiO_2 doped with 1.5 mg FK209 is ranging between (11–15)%. This indicates that devices fabricated with 2.5-mg concentration of FK209 have higher reproducibility compared with other concen-

tration. It is worth noticing that the 2.5-mg concentration produced larger grains size and smoother surfaces. Consequently, the 2.5 mg FK209 concentration produced higher conductivity films with slightly better transparency. As a result, the PCE of these devices were higher and more reproducible.

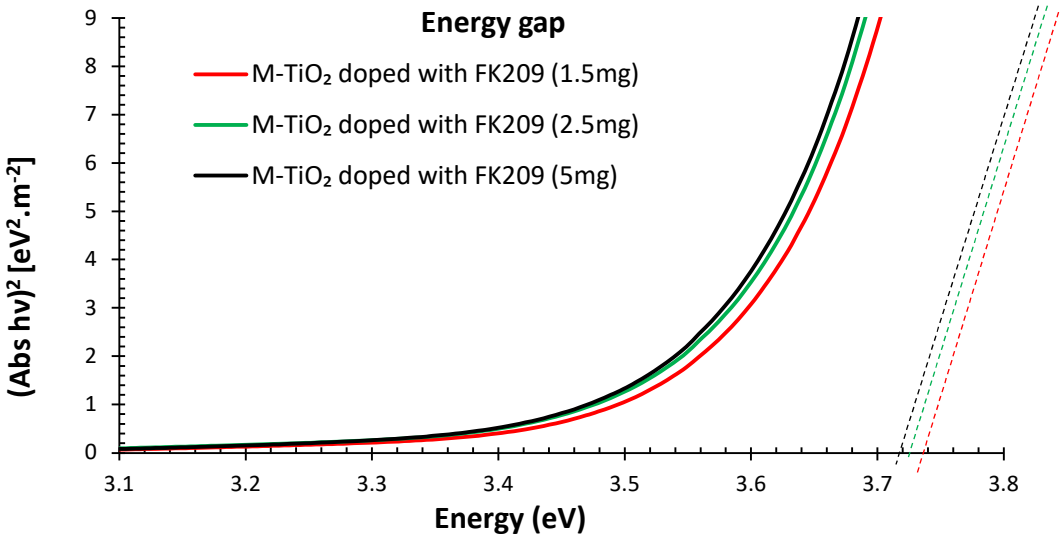

Figure 15. Energy gap of M-TiO_2 doped with various concentrations of FK209 (1.5 mg, 2.5 mg and 5 mg) using Tauc plot. Dotted lines represent the tangent to the slope for each plot.

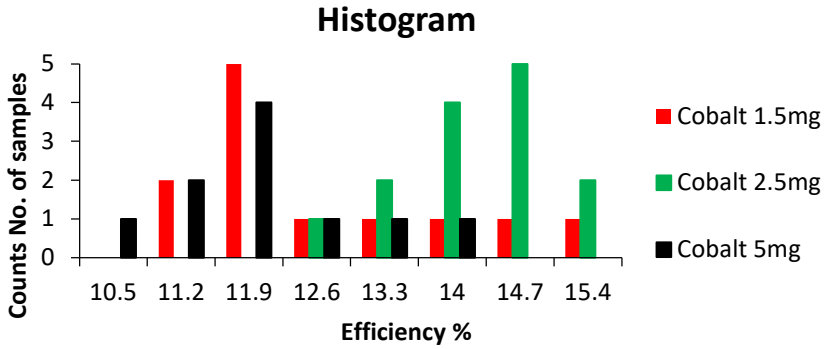

Figure 16. Statistical histogram of the PCE measured over 30 fabricated solar cells. The ETL was fabricated using C-TiO_2 prepared using DC-sputtering and M-TiO_2 doped with various concentrations of FK209.

One of the main challenges facing the wide spread use of perovskite solar cells is their long time stability and it was reported in a number of articles [16,32]. The stability of perovskite or the deterioration in performance of perovskite is due to changing in crystal structure, which was noticed when exposing the material to high temperature, moisture, oxygen and prolonged illumination [33]. Solvents and additives used in the HTL and ETL layers can also influence the stability of perovskite cells [33,34].

Some of the reported efficiency of perovskite exhibited deterioration by up to 20% after 200 h [9] and some deteriorated by 8% after 20 days [34]. In our devices, the stability of the fabricated devices were studied by measuring the solar cell efficiency over an extended period of 40 weeks while the devices were kept under ambient laboratory conditions of 50% humidity and 25 °C temperature. The efficiency was measured using sunlight simulator as described in Section 3.4. The illuminated J–V characteristics were monitored over 40 weeks by repeating the characterization every 2 weeks period then at every month in an ambient laboratory conditions. Figure 17 illustrates the stability test deduced from the forward and backward J-V scan conducted to measure the PSCs efficiency. The drop in efficiency was around 20% for samples prepared using M-TiO_2 doped with FK209, while the drop was

27% for control samples prepared without doping over the same period of 40 weeks. We reported previously that the stability could be improved by using green solvents such as Ethanol rather than using Acetonitrile (ACN) [35]. It is known that ACN is toxic and can accelerate the deterioration of the perovskite films [34]. Ethanol and Isopropyl alcohol (IPA) have been suggested as alternative solvents in dissolving FK209 cobalt and lithium TFSI salt respectively. These solvents have resulted in improve stability, device performance and slowed down the degradation of the perovskite films [34,35]. In addition, in this work, Cesium Lead Halide Perovskite is utilized rather than MAI based perovskite as it offers better stability [36].

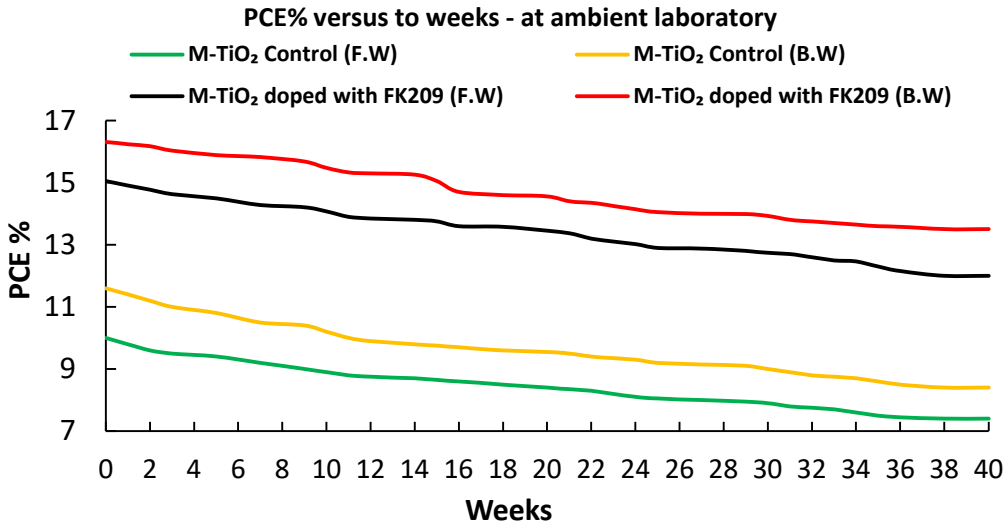

Figure 17. Device stability testing by measuring variations in the efficiency of the perovskite solar cells measured over 40 weeks period in weekly intervals. Devices were kept in ambient laboratory and tested under AM1.5, 100 mW/cm^2 illumination using ABET sunlight simulators with reference cell as a control.

4. Conclusions

In summary, FK209 cobalt TFSI and lithium TFSI salt were investigated as dopant for the mesoporous TiO_2 in the electron transport layer. The concentration of the FK209 cobalt was varied from 1.5 mg to 5 mg. It was found that the ETL with M-TiO_2 doped with FK209 cobalt at a 2.5-mg concentration achieved highest efficiency due to its transparency, good conductivity, high mobility and low surface roughness compared with M-TiO_2 doped with lithium. From the optical characterization, it was found that the transparency of the M-TiO_2 doped with FK209 is around 90% and the energy gap was 3.59 eV. The M-TiO_2 doped with FK209 has a minimal surface roughness and low contact angle (hydrophilic) as compared with undoped control sample. The perovskite film deposited on M-TiO_2 doped with FK209 has a lower PL intensity indicating faster charge extraction. The measured lifetime of the perovskite films deposited on the M-TiO_2 doped with FK209 was 115.8 ns, which is about 2.5% longer than the perovskite films deposited on the M-TiO_2 doped with lithium. The average efficiency of the perovskite solar cell deposited on the C-TiO_2 and M-TiO_2 doped with FK209 electron transport layer is 15.6%. This is 44% higher than the PSCs deposited on undoped M-TiO_2. The FK209 cobalt doping also offers improved stability compared to lithium doping or undoped M-TiO_2 control device. The stability of the devices was monitored over 40 weeks period under ambient laboratory conditions of 50% humidity and 25 °C temperature. The perovskite solar cells exhibit a 20% drop in efficiency over the 40 weeks testing period when using M-TiO_2 ETL doped with FK209 and a drop of 27% for the undoped M-TiO_2. This study demonstrated that using FK209 cobalt with 2.5-mg concentration to dope the M-TiO_2 provides high efficiency PSC devices with improved stability and reproducibility.

Author Contributions: A.H. conceived the original idea, performed the experimental work and wrote draft of the manuscript; R.J.R. supervised the photoluminescence and spectroscopy measurements; M.M.A. supervised the work, performed analysis and contributed to the discussion of the results and revised the manuscript. All authors have read and agreed to the published version of the manuscript.

Funding: A.H., acknowledge the UC Doctoral Scholarship funding, University of Canterbury, New Zealand. M.M.A and R.J.R acknowledge the support of the MacDiarmid Institute for Advanced Materials and Nanotechnology, New Zealand.

Institutional Review Board Statement: Not applicable.

Informed Consent Statement: Not applicable.

Data Availability Statement: Not applicable.

Acknowledgments: The authors would like to thank Linda Chen, Gary Turner and Helen Devereux from the Nanofabrication Laboratory, University of Canterbury, New Zealand for providing technical assistance.

Conflicts of Interest: The authors declare no conflict of interest.

References

1. Kojima, A.; Teshima, K.; Shirai, Y.; Miyasaka, T. Organometal Halide Perovskites as Visible-Light Sensitizers for Photovoltaic Cells. *J. Am. Chem. Soc.* **2009**, *131*, 6050–6051. [CrossRef] [PubMed]
2. Jeong, J.; Kim, M.; Seo, J.; Lu, H.; Ahlawat, P.; Mishra, A.; Yang, Y.; Hope, M.A.; Eickemeyer, F.T.; Kim, M.; et al. Pseudo-Halide Anion Engineering for α-FAPbI3 Perovskite Solar Cells. *Nature* **2021**, *592*, 381–385. [CrossRef] [PubMed]
3. Seo, J.Y.; Uchida, R.; Kim, H.S.; Saygili, Y.; Luo, J.; Moore, C.; Kerrod, J.; Wagstaff, A.; Eklund, M.; McIntyre, R.; et al. Boosting the Efficiency of Perovskite Solar Cells with CsBr-Modified Mesoporous TiO_2 Beads as Electron-Selective Contact. *Adv. Funct. Mater.* **2018**, *28*, 1705763. [CrossRef]
4. Ke, W.; Fang, G.; Wang, J.; Qin, P.; Tao, H.; Lei, H.; Liu, Q.; Dai, X.; Zhao, X. Perovskite Solar Cell with an Efficient TiO_2 Compact Film. *ACS Appl. Mater. Interfaces* **2014**, *6*, 15959–15965. [CrossRef] [PubMed]
5. Du, Y.; Cai, H.; Wu, Y.; Xing, Z.; Li, Z.; Xu, J.; Huang, L.; Ni, J.; Li, J.; Zhang, J. Enhanced Planar Perovskite Solar Cells with Efficiency Exceeding 16% via Reducing the Oxygen Vacancy Defect State in Titanium Oxide Electrode. *Phys. Chem. Chem. Phys.* **2017**, *19*, 13679–13686. [CrossRef] [PubMed]
6. Gu, X.; Wang, Y.; Zhang, T.; Liu, D.; Zhang, R.; Zhang, P.; Wu, J.; Chen, Z.D.; Li, S. Enhanced Electronic Transport in Fe^{3+}-Doped TiO_2 for High Efficiency Perovskite Solar Cells. *J. Mater. Chem. C* **2017**, *5*, 10754–10760. [CrossRef]
7. Liu, D.; Li, S.; Zhang, P.; Wang, Y.; Zhang, R.; Sarvari, H.; Wang, F.; Wu, J.; Wang, Z.; Chen, Z.D. Efficient Planar Heterojunction Perovskite Solar Cells with Li-Doped Compact TiO_2 Layer. *Nano Energy* **2017**, *31*, 462–468. [CrossRef]
8. Saliba, M.; Correa-Baena, J.-P.; Wolff, C.M.; Stolterfoht, M.; Phung, N.; Albrecht, S.; Neher, D.; Abate, A. How to Make over 20% Efficient Perovskite Solar Cells in Regular (n–i–p) and Inverted (p–i–n) Architectures. *Chem. Mater.* **2018**, *30*, 4193–4201. [CrossRef]
9. Sidhik, S.; Cerdan Pasarán, A.; Esparza, D.; López Luke, T.; Carriles, R.; De La Rosa, E. Improving the Optoelectronic Properties of Mesoporous TiO_2 by Cobalt Doping for High-Performance Hysteresis-Free Perovskite Solar Cells. *ACS Appl. Mater. Interfaces* **2018**, *10*, 3571–3580. [CrossRef]
10. Giordano, F.; Abate, A.; Correa Baena, J.P.; Saliba, M.; Matsui, T.; Im, S.H.; Zakeeruddin, S.M.; Nazeeruddin, M.K.; Hagfeldt, A.; Graetzel, M. Enhanced Electronic Properties in Mesoporous TiO_2 via Lithium Doping for High-Efficiency Perovskite Solar Cells. *Nat. Commun.* **2016**, *7*, 10379. [CrossRef]
11. Ren, G.; Li, Z.; Wu, W.; Han, S.; Liu, C.; Li, Z.; Dong, M.; Guo, W. Performance Improvement of Planar Perovskite Solar Cells with Cobalt-Doped Interface Layer. *Appl. Surf. Sci.* **2020**, *507*, 145081. [CrossRef]
12. Kim, M.; Choi, I.W.; Choi, S.J.; Song, J.W.; Mo, S.I.; An, J.H.; Jo, Y.; Ahn, S.J.; Ahn, S.K.; Kim, G.H.; et al. Enhanced Electrical Properties of Li-Salts Doped Mesoporous TiO_2 in Perovskite Solar Cells. *Joule* **2021**, *5*, 659–672. [CrossRef]
13. Alkahtani, M.; Almuqhim, A.A.; Qasem, H.; Alsofyani, N.; Alfahd, A.; Alenzi, S.M.; Aljuwayr, A.; Alzahrani, Y.A.; Al-Badri, A.; Alotaibi, M.H.; et al. Lithium-Based Upconversion Nanoparticles for High Performance Perovskite Solar Cells. *Nanomaterials* **2021**, *11*, 2909. [CrossRef]
14. Alkahtani, M.; Qasem, H.; Alenzi, S.M.; Alsofyani, N.; Alfahd, A.; Aljuwayr, A.; Hemmer, P.R. Electrodeposition of Lithium-Based Upconversion Nanoparticle Thin Films for Efficient Perovskite Solar Cells. *Nanomaterials* **2022**, *12*, 2115. [CrossRef] [PubMed]
15. Hayali, A.; Alkaisi, M.M. High Efficiency Perovskite Solar Cells Using DC Sputtered Compact TiO_2 electron Transport Layer. *EPJ Photovolt.* **2021**, *12*, 8. [CrossRef]
16. Chavan, R.D.; Yadav, P.; Nimbalkar, A.; Bhoite, S.P.; Bhosale, P.N.; Kook Hong, C. Ruthenium Doped Mesoporous Titanium Dioxide for Highly Efficient, Hysteresis-Free and Stable Perovskite Solar Cells. *Sol. Energy* **2019**, *186*, 156–165. [CrossRef]
17. Wang, S.; Ma, Z.; Liu, B.; Wu, W.; Zhu, Y.; Ma, R.; Wang, C. High-Performance Perovskite Solar Cells with Large Grain-Size Obtained by Using the Lewis Acid-Base Adduct of Thiourea. *Sol. RRL* **2018**, *2*, 1800034. [CrossRef]

18. Nie, W.; Tsai, H.; Asadpour, R.; Neukirch, A.J.; Gupta, G.; Crochet, J.J.; Chhowalla, M.; Tretiak, S.; Alam, M.A.; Wang, H. High-Efficiency Solution-Processed Perovskite Solar Cells with Millimeter-Scale Grains. *Science* **2015**, *347*, 522–526. [CrossRef]
19. Sherkar, T.S.; Momblona, C.; Gil-Escrig, L.; Ávila, J.; Sessolo, M.; Bolink, H.J.; Koster, L.J.A. Recombination in Perovskite Solar Cells: Significance of Grain Boundaries, Interface Traps, and Defect Ions. *ACS Energy Lett.* **2017**, *2*, 1214–1222. [CrossRef]
20. Wu, T.; Wu, J.; Tu, Y.; He, X.; Lan, Z.; Huang, M.; Lin, J. Solvent Engineering for High-Quality Perovskite Solar Cell with an Efficiency Approaching 20%. *J. Power Sources* **2017**, *365*, 1–6. [CrossRef]
21. Ghobadi, N. Band Gap Determination Using Absorption Spectrum Fitting Procedure. *Int. Nano Lett.* **2013**, *3*, 2–5. [CrossRef]
22. Kumi-Barimah, E.; Penhale-Jones, R.; Salimian, A.; Upadhyaya, H.; Hasnath, A.; Jose, G. Phase Evolution, Morphological, Optical and Electrical Properties of Femtosecond Pulsed Laser Deposited TiO_2 Thin Films. *Sci. Rep.* **2020**, *10*, 10144. [CrossRef] [PubMed]
23. Niu, B.; Wang, X.; Wu, K.; He, X.; Zhang, R. Mesoporous Titanium Dioxide: Synthesis and Applications in Photocatalysis, Energy and Biology. *Materials* **2018**, *11*, 1901. [CrossRef] [PubMed]
24. Li, Y.; Zhang, T.; Xu, F.; Wang, Y.; Li, G.; Yang, Y.; Zhao, Y. CH3NH3Cl Assisted Solvent Engineering for Highly Crystallized and Large Grain Size Mixed-Composition (FAPbI3)0.85(MAPbBr3)0.15 Perovskites. *Crystals* **2017**, *7*, 272. [CrossRef]
25. Prasanna, R.; Gold-Parker, A.; Leijtens, T.; Conings, B.; Babayigit, A.; Boyen, H.G.; Toney, M.F.; McGehee, M.D. Band Gap Tuning via Lattice Contraction and Octahedral Tilting in Perovskite Materials for Photovoltaics. *J. Am. Chem. Soc.* **2017**, *139*, 11117–11124. [CrossRef]
26. Yan, K.; Chen, J.; Ju, H.; Ding, F.; Chen, H.; Li, C.Z. Achieving High-Performance Thick-Film Perovskite Solar Cells with Electron Transporting Bingel Fullerenes. *J. Mater. Chem. A* **2018**, *6*, 15495–15503. [CrossRef]
27. Kim, D.I.; Lee, J.W.; Jeong, R.H.; Boo, J.H. A High-efficiency and Stable Perovskite Solar Cell Fabricated in Ambient Air Using a Polyaniline Passivation Layer. *Sci. Rep.* **2022**, *12*, 697. [CrossRef]
28. Park, M.; Kim, J.Y.; Son, H.J.; Lee, C.H.; Jang, S.S.; Ko, M.J. Low-Temperature Solution-Processed Li-Doped SnO_2 as an Effective Electron Transporting Layer for High-Performance Flexible and Wearable Perovskite Solar Cells. *Nano Energy* **2016**, *26*, 208–215. [CrossRef]
29. Levine, I.; Nayak, P.K.; Wang, J.T.W.; Sakai, N.; Van Reenen, S.; Brenner, T.M.; Mukhopadhyay, S.; Snaith, H.J.; Hodes, G.; Cahen, D. Interface-Dependent Ion Migration/Accumulation Controls Hysteresis in MAPbI3 Solar Cells. *J. Phys. Chem. C* **2016**, *120*, 16399–16411. [CrossRef]
30. Liu, U.P.; Wang, W.; Liu, S.; Yang, H.; Shao, Z. Fundamental Understanding of Photocurrent Hysteresis in Perovskite Solar Cells. *Adv. Energy Mater.* **2019**, *9*, 1803017. [CrossRef]
31. Habisreutinger, S.N.; Noel, N.K.; Snaith, H.J. Hysteresis Index: A Figure without Merit for Quantifying Hysteresis in Perovskite Solar Cells. *ACS Energy Lett.* **2018**, *3*, 2472–2476. [CrossRef]
32. Tai, M.; Lau, C.F.J.; Lin, H.; Wang, Z. Advances in Phase Stability of Cesium Lead Halide Perovskites. *Sol. RRL* **2020**, *4*, 2000495. [CrossRef]
33. Zhao, X.; Park, N.G. Stability Issues on Perovskite Solar Cells. *Photonics* **2015**, *2*, 1139–1151. [CrossRef]
34. Zou, J.; Wu, J.; Sun, W.; Zhang, M.; Wang, X.; Yuan, P.; Zhu, Q.; Yin, J.; Liu, X.; Yang, Y. Solvent Engineering of LiTFSI towards High-Efficiency Planar Perovskite Solar Cells. *Sol. Energy* **2019**, *194*, 321–328. [CrossRef]
35. Hayali, A.; Alkaisi, M.M. Solvent Engineering of FK209 Cobalt and Lithium for High-Efficiency Perovskite Solar Cells. In Proceedings of the 2021 IEEE 48th Photovoltaic Specialists Conference (PVSC), Fort Lauderdale, FL, USA, 20–25 June 2021; pp. 2253–2259. [CrossRef]
36. Beal, R.E.; Slotcavage, D.J.; Leijtens, T.; Bowring, A.R.; Belisle, R.A.; Nguyen, W.H.; Burkhard, G.F.; Hoke, E.T.; McGehee, M.D. Cesium Lead Halide Perovskites with Improved Stability for Tandem Solar Cells. *J. Phys. Chem. Lett.* **2016**, *7*, 746–751. [CrossRef]